Evaluation of a Ground-Based Sky Camera System for Use in Surface Irradiance Measurement

JEFF SABBURG

Centre for Astronomy and Atmospheric Research, University of Southern Queensland, Toowoomba, Australia, and Centre for Medical and Health Physics, Queensland University of Technology, Brisbane, Australia

JOE WONG

Centre for Medical and Health Physics, Queensland University of Technology, Brisbane, Australia

(Manuscript received 17 April 1998, in final form 20 August 1998)

ABSTRACT

This paper describes the evaluation of a ground-based sky camera system for studying the effect of clouds on the level of the ambient ultraviolet radiation. The system has been developed for research in the characterization of the effect of clouds around the sun. It is the first sky camera system to be used for the assessment of cloud conditions in the vicinity of the sun, rather than a whole-sky assessment. The system features a sun-tracking sky camera with an integrated measurement of horizontally received radiation at the same location. The image-processing algorithm uses solar radiation readings to reduce reflections from the sun on the camera system being mistaken for cloud in the images. Cloud amount was estimated in an angular region of between 12.5° and 37.5° around the sun. The algorithm also estimates the amount of solar obstruction by cloud (sun not covered, partially or totally covered). The system was evaluated during September 1997 at Toowoomba, Australia (27.6°S latitude). Compared to manual assessment of 592 images, 76.5% were identified correctly by the algorithm for the degree of solar obstruction and 81.9% for cloud amount. The behavior of ultraviolet radiation levels with cloud conditions is discussed.

1. Introduction

Satellite cloud data may be used in conjunction with radiation models to map ultraviolet radiation (UVR) in a geographical region (Nunez et al. 1994). No satellite-based whole-sky camera has been used to study the effect of cloud amount on UVR at ground level. Borkowski et al. (1977) and Schafer et al. (1996) employed ground-based whole-sky cameras to study cloud effects on UVR at ground level. In both studies the degree of solar obstruction and whole-sky cloud amount were determined visually (not automatically) from the images by subjective methods. Presumably the cloud amount in the vicinity of the sun produces the most important effect on the level of ambient UV. At the present time there has been no reported study of the measurement of cloud properties in the vicinity of the sun using an automated satellite- or ground-based sky camera system. Cloud images in the vicinity of the sun can be recorded automatically with a sun-tracking camera. In order to process a vast number of images of cloud, it is desirable to automate the image analysis process.

Goodman and Henderson-Sellers (1988) and Wooldridge (1993) review the major approaches to automatic cloud measurement for meteorological purposes. Goodman and Henderson-Sellers (1988) concentrate on satellite techniques and Wooldridge (1993) reviews ground-based systems. Wooldridge (1993) describes the development and evaluation of an automated whole-sky camera system to estimate cloud amount. Discrimination into cloud or clear sky was made on the basis of the difference between the measured pixel brightness level and the expected brightness level of that pixel in the clear sky and the position of the pixel in relation to the sun. Davis et al. (1992) used color slides as a source of cloud images. They employed a threshold method to determine the cloud amount of the images obtained from the color slides. Any pixel values below two chosen thresholds were taken to be cloud, and pixel values above were taken to be sky. Because Wooldridge found only qualitative agreement compared to visual observations of cloud when applying his technique to measuring cloud amount, a combination of both of these approaches has been adopted for use in the sky camera presented in this paper. The difference is that the comparison of image pixel to that expected in a clear sky

Corresponding author address: Mr. Jeff Sabburg, Department of Physical and Biological Sciences, University of Southern Queensland, Toowoomba, Queensland 4350, Australia.
E-mail: sabburg@usq.edu.au

FIG. 1. Radiation measurement (datalogger in foreground) and sky image capture subsystem (power supply, camera, and stepper motor housing in the background).

(Wooldridge 1993) was modified to incorporate a correlation technique to determine the degree of solar obstruction. The threshold method of Davis et al. (1992) was adapted by using a nonlinear approach to measure cloud amount. This adaptation reduced the problem that Davis et al. found of incorrectly identifying weak cloud edges.

The present paper presents the evaluation of the automated, ground-based, sun-centered sky camera (SCSC) system for cloud assessment for the period of September 1997, solar zenith angle (SZA) 53.2° to 23.9° between 0900 and 1500 LT. Details of the requirement for the camera are presented in Sabburg and Wong (1997). This evaluation is used to illustrate the potential for the SCSC to automatically retrieve information about solar obstruction and cloud amount data. The evaluation also includes a brief discussion about the use of the data for studying the effects of the cloud on the UV radiation at the ground level. The topic will be illustrated with available data. Additional papers will provide more detailed analyses of future data.

2. Instrumentation

The SCSC system consists of three subsystems: a radiation measurement unit (datalogger shown in Fig. 1), a sky image capture subsystem (camera and stepper motors also shown in Fig. 1), and an image analysis computer. A control computer that contains a frame-grabber card (Digital Vision 1992) is connected to the camera [charged coupled device (CCD) supplied by ISSCO]. The stepper motor driver (supplied by Arrick Robotics 1995) is connected to the Centronics printer port of the computer. The datalogger of the radiation measurement unit is connected to the RS232 port of the computer. Images and data are sent offline via an ethernet card to the image analysis computer. This computer runs the image-processing algorithm that is written using the commercial computer package MATLAB and the associated image-processing toolbox (Thompson and Shure 1995).

The radiation measurement unit and most of the sky image capture subsystem are located approximately 11 m above the ground on a flat corrugated roof of a three-story building at the campus of the University of Southern Queensland (USQ) in Toowoomba (27.6°S latitude, 696 m above sea level) (Fig. 1). The distance between the radiation sensors and camera is approximately 5.7 m. This location has essentially 360° unobstructed views for 10° or more above the horizon, an approximate uniform UVR albedo of 0.1, and relatively nonpolluted skies. The radiation measurement unit comprises a commercial datalogger (supplied by Monitor Sensors 1989) and three solar detectors (UVB, 280–320 nm; UVA, 320–400 nm; sunlight, 400–950 nm) for monitoring the 6-min average UVB, UVA, and total sunlight, respectively. These data together with the date and the time are sent to the controlling computer at 6-min intervals.

The UV data was calibrated at noon during the measurement period by comparison of the irradiances to those measured by a spectroradiometer with calibration traceable to the primary Australian standard lamp housed at the National Measurement Laboratory (Wong et al. 1995). Daily total column ozone in Dobson units (DUs) near the site of cloud measurements was recorded by a Dobson spectrophotometer. The uncertainty of the data was estimated to be within ±3%. As the ozone levels were considered constant throughout the day, the data represent the daily average of the ozone level.

The sky image capture subsystem comprised a camera and a stepper motor control. The camera consisted of a standard color video camera (½″ CCD), with shutter set to 1/125 s and a wide-angle lens (½″ CS mount, *F*16, focus set to infinity). One stepper motor was used to turn a filter wheel assembly that was located above the camera lens (Fig. 2). This assembly consisted of six apertures (55-mm diameter), equally spaced at 60° [opaque, clear, ×2, ×4, ×8, neutral density, and red filter]. The first aperture was opaque (coated with aluminium foil) and ensured that the sun's rays did not damage the CCD chip of the camera. The clear filter was made of Perspex. The remaining filters were obtained from a typical 35-mm camera set.

The second motor was geared to point the camera in the direction of the sun in an east–west direction. Two components of the sky image capture system (the camera and the filter wheel stepper motor assembly), were housed in a weatherproof portable Peltier refrigerator (supplied by Kookaurra Pty. Ltd.), with a circular glass

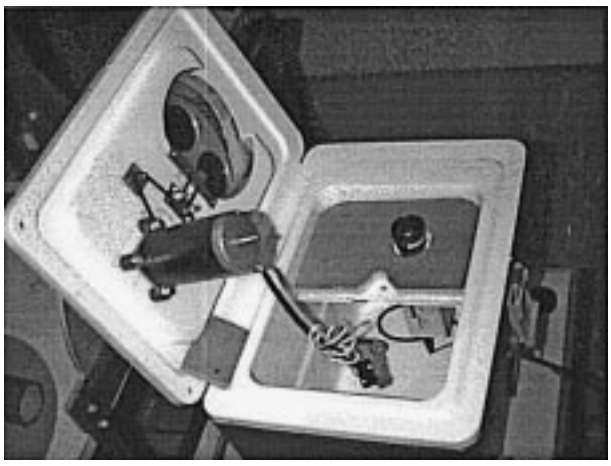

FIG. 2. Stepper motor used to turn a filter wheel assembly, which is located above the camera lens when the lid is closed. This Peltier-cooled housing is also shown in the background of Fig. 1.

opening (145-mm diameter) for image capture (Fig. 2). The Peltier was used to keep the camera in an operating temperature range below 40°C. The refrigerator was supported by a ''cradle'' attached to a frame that was positioned to allow the sun and the surrounding sky to appear in the field of view (FOV) of the camera (75° east–west and 98° north–south). The power supply for the camera and Peltier were housed in an adjacent semi-weatherproof box (Fig. 1).

3. Instrument control methodology

The control program was designed to control the two stepper motors. Initially the camera was pointed at the sun on power-up by one of the stepper motors. This initial setup was achieved by obtaining the time of day from the datalogger (synchronizing the computer clock to this time) and waiting until the stepper motor positioned itself in 0.06° steps either in the clockwise or anticlockwise direction. This was based on using the equation of time (Nautical Almanac Office 1985) to set the camera in an appropriate position at local noon and a movement of 15° h^{-1} from this position. The motor was geared at a ratio of 1:15 with a minimum step of 0.9°. Thus it can track the sun every 14.4 s. The altitude angle of the camera was manually adjusted at the end of each week by approximately 2°. This was necessary to keep the sun in the center of the FOV of the camera in a north–south direction.

Once the camera was in position, the program waited for a 6-min period during which the datalogger sent weather data to the control computer (approximately 100 Mbytes per month). Two minutes later the camera was moved an appropriate number of steps in a clockwise direction to maintain the sun in the center of the FOV of the camera (±20 pixels). The program then consecutively rotated the filter wheel by 60° storing three of the five available graphical interchange format (GIF) images (clear, ×4, and red) of the clouds. Each GIF image was 200 × 320 pixels and the weather data were stored as sequential data files. Thus for each 6 min, a data file and three image files were stored.

This procedure was repeated between 0900 and 1500 LT each day or until user intervention occurred. At 1500 LT the camera was returned to the vertical position and the program ended. The Peltier refrigerator and camera was turned off at 1630 LT by a digital timer, enabling the interior of the refrigerator to further cool down. They were turned on again at 0830 LT the next day. The controlling computer and the stepper motor driver unit were also controlled by a separate digital timer to switch on at 0850 LT and off again at 1710 LT. At the end of each month, the data that had been stored on the control computer were transferred to the image analysis computer for batch processing over the weekend period. The execution time was approximately 1 min per image.

4. Image analysis methodology

The image-processing algorithm used the three stored images in different ways. The first and last images were converted from an indexed format, with corresponding colormap, to a red green blue (RGB) format, the first with 100% hue and saturation and the last with 0% hue and 100% saturation. The second image was converted from indexed to a 256 grayscale format (Thompson and Shure 1995, p. 2-126, 2-127). The green component of the red filtered RGB image (to be referred to as image 1) was found to be the most appropriate color component in identifying the sun's location in relatively cloudy conditions, as the sun's disk was of maximum contrast. The red component of the RGB clear aperture image (image 3) was used in identifying cloud pixel in relatively cloudy conditions when averaged with the grayscale ×4 ND filter image (image 2). This averaged image provided optimum contrast between cloud and sky. Image 2 was also used for locating the sun and identifying cloud in all other sky conditions. All images were relatively free of noise, except for the presence of horizontal lines in some cases of image 1. These lines were most likely due to electrical interference.

As well as the three images, information from the solar radiation sensor was used to determine when to select image 3 by comparing the solar radiation data corresponding to each image to that corresponding to a selected clear-sky or reference image (RI). The solar radiation data was also used in decisions relating to the degree of obstruction of the sun. The initial decision of the degree of solar obstruction was based on a comparison of the chosen image with that of the RI. This was then used for comparison with all images to be analyzed (ITBA) for that month. The level of solar radiation was also used to adjust the threshold values. A threshold (or comparison value) was used for deter-

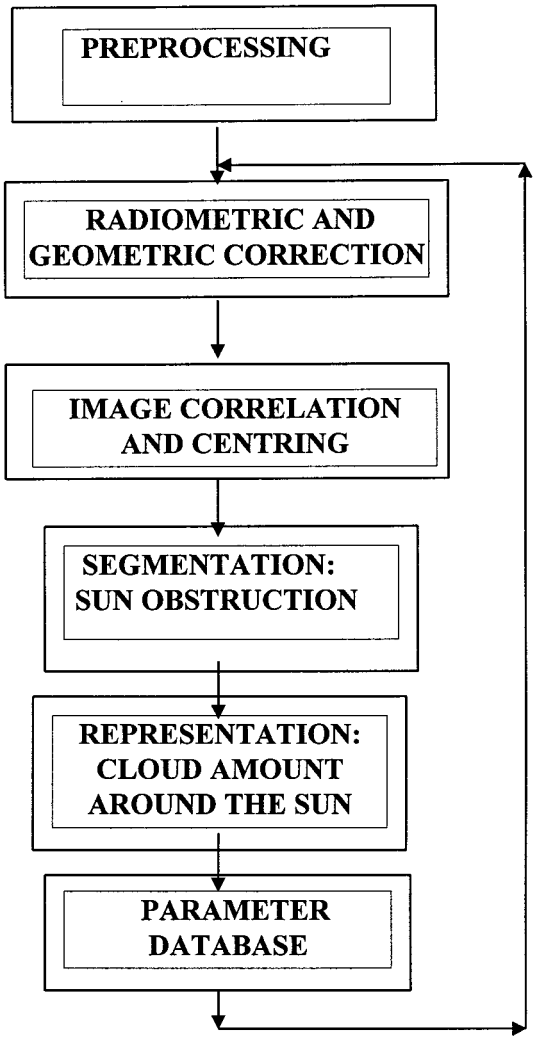

FIG. 3. Block diagram of the main steps of the image analysis algorithm for the SCSC.

mining which image pixel is cloud or sky. Thresholding is the process through which a pixel is identified to be either free of cloud or totally filled with cloud, depending on whether the measured radiance is above or below the threshold values. This was achieved by converting the grayscale image to a binary image based on the image pixel values being higher or lower than the threshold value. Reflection from the sun on the camera system sometimes caused an error when identifying the cloud in the images. For a selected range of solar radiation readings the image threshold value was increased to reduce these reflections from the sun on the camera system being mistaken as cloud.

Under special circumstances it was possible to determine the cloud type: either cirrus (Ci) or other cloud. This was determined by the standard deviation (SD) of values of the threshold cloud explained below. This SD was also used in determining the degree of obstruction of the sun when Ci clouds were involved.

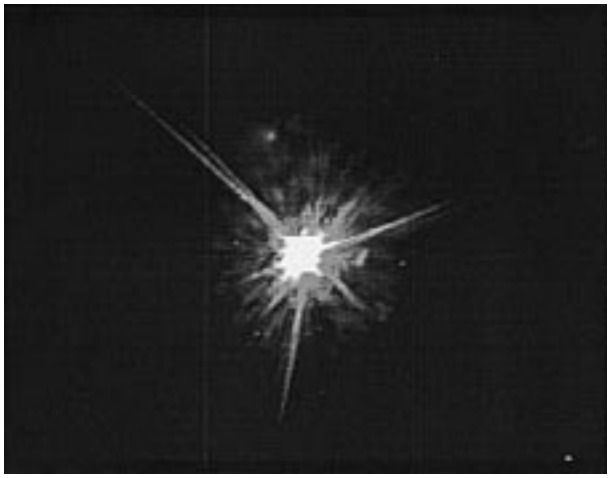

FIG. 4. Centered 256 grayscale reference image (clear sky, 1159 LT 9 Sep 1997), 200 × 320 pixels.

Figure 3 shows the block diagram of the essential steps of the image analysis algorithm that has been developed for the SCSC. To develop the algorithm 829 sky images were collected during the first 15 days of September 1997. Each image was visually inspected for the properties of the degree of solar obstruction and for an estimate of the cloud amount around the sun. Repetitive changes (sometimes called ''supervized'' training) were made to the algorithm based on the computer versus visual results. This process improved the false alarm rate of detection of the cloud properties. The expectation is that when more images are used in supervised training an increase in the accuracy of the algorithm when applied to new image datasets will occur. The following is a brief description of each of these steps.

a. Preprocessing

Initially the program checked for any nonreadable images that may have occurred and for the correct structure and sequence of image and data files. This was achieved by attempting to read each GIF image successfully, followed by checking the sequence of times that the images and data were stored. Next, a manual selection of the RI was made for the month. This was chosen typically midway during the month and around noon to correspond to the day of the UV sensor calibration. The sun's location with respect to the center of the image and the corresponding solar radiation reading were noted. The image pixel was then translated until the sun was positioned at the center of the RI (Fig. 4).

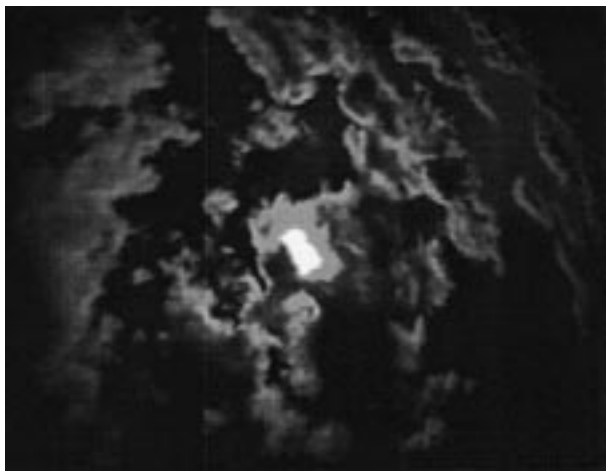

FIG. 5. Image 2: 256 Grayscale 200 × 256 pixel image of cloudy sky (1041 LT 11 Sep 1997). This corresponds to data point 15 of Fig. 8. Disk obscured and 79% cloud cover in FOV.

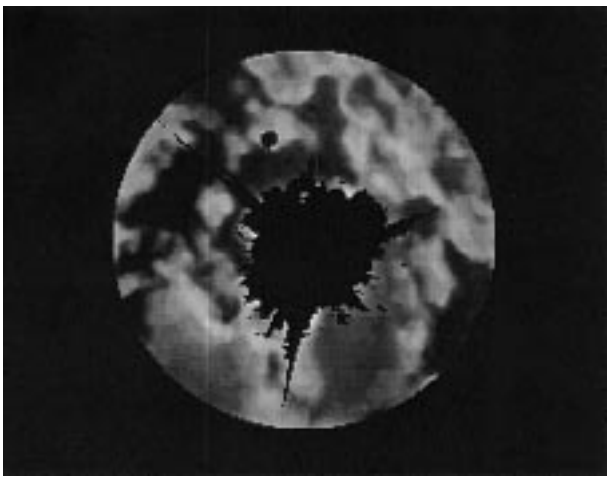

FIG. 6. Sun mask from Fig. 4 and a 70° FOV mask applied to Fig. 5 averaged with image 1.

b. Radiometric and geometric correction

From laboratory tests of the SCSC, it was determined that the image geometry of a circular disk was approximately equal in area (±1.3%) after an image resizing from 200 × 320 to 200 × 256 pixels. Bilinear interpolation was used to perform the resizing. This fits a linear surface through the values of the four closest pixels. The resizing was applied to images 1, 2, and 3 of the ITBA (Fig. 5).

c. Image correlation and centering

A correlation method based on a comparison with the RI (image 2 or 3) was developed using the following algorithm. The correlation coefficient r (Thompson and Shure 1995) was defined as

$$r = \frac{\sum_{n_1}\sum_{n_2} A(n_1, n_2)B(n_1, n_2)}{\sqrt{\sum_{n_1}\sum_{n_2} A^2(n_1, n_2)\sum_{n_1}\sum_{n_2} B^2(n_1, n_2)}}, \quad (1)$$

where A and B are the RI and ITBA, respectively. After ±20 pixel shifts in the m and n directions of the RI, plus an additional ±5° rotations, the m, n, and rotation values of the highest correlations were used to center the ITBA, except in cases where the sun was totally obscured. The normalized solar radiation (NSR) value was calculated as the ratio of the corresponding ITBA/RI values. The mean brightness of the image (IMB) was determined (Thompson and Shure 1995) for the case of very bright clouds when the sun was actually blocked.

d. Degree of solar obstruction and cloud amount around the sun

A circular mask of 30° FOV (radius of 35 pixels) was applied to image 2 of both the RI and the ITBA. This mask highlighted the mean brightness around the sun (SMB). The indices defined in the preceding section were determined and they were used for classification of the images. The criteria for the application of the mask (Thompson and Shure 1995, p. 2–98) was obtained by the training program using the 829 images as described in the introduction to section 4. The degree of solar obstruction algorithm is summarized in appendix A. The last ''disk obscured'' (DO) condition also indicated Ci cloud.

A circular mask of 70° FOV (radius of 80 pixels) was then applied to the ITBA, as this is the maximum FOV in all directions of the video camera. This ensured that all pixels in this masked area had been calibrated. Second, the sun mask described above was subtracted from images 1 and 2 of the ITBA. This was achieved by the use of masked filtering using a filter consisting of 9 × 9 zeros (Thompson and Shure 1995, p. 2–138). This sun mask takes up 8.5% of the image area, with most area in a 10° FOV (Fig. 6). Next, thresholding of the remaining pixel to either cloud or clear sky was applied (Fig. 7). The thresholding levels used in this paper were varied according to the degree of solar obstruction of the image (which included solar radiation values), as well as depending on the IMB. The threshold conditions for cloud amount determination are summarized in appendix B. The average of images 1 and 2 were found after a (5 × 3) median filter was applied (Thompson and Shure 1995, p. 2-136, 2-137). This was a nonlinear filter that computes the value centered under the filter for each local $m \times n$ neighborhood to reduce the general noise level, in particular, horizontal lines.

FIG. 7. Thresholding of Fig. 6 based on the state of the sun's disk.

TABLE 1. Results of comparison between visual and algorithm-derived cloud parameters for 592 images.

Parameter	Visual	Algorithm			Error (%)
State of Sun					
DO	251			219	12.7
		DPO	29		
		DNO	3		
DPO	118			46	61.0
		DO	43		
		DNO	29		
DNO	223			188	15.7
		DO	6		
		DPO	29		
Total	592		(139)	453	23.5
Cloud Category					
100%–80%	244			233	4.5
80%–50%	91			15	83.5
50%–1%	105			86	18.1
1%–0%	152			151	0.7
Total	592			485	18.1

All of the above decisions were based on the premise that for dark scenes or dark clouds, lower thresholds are required and for bright scenes or thin clouds, higher thresholds are needed. This kept under- or overestimation of cloud amount around the sun to a minimum. The area of the cloud was then determined in the region of interest (ROI). This ROI is that area not occupied by the sun mask and inside the 75° FOV mask. The area was measured using 2×2 pixel patterns, called bit quads. There are six categories of bit quads. The bit quads are grouped in the image based on their pattern categories. The estimate is based on a weighted sum of the number of each bit quad pattern found in the image, with each pattern having a different weighting factor (Thompson and Shure 1995, p. 2–14). Mean fractional cloud amount was estimated by counting the number of cloudy pixel within a region. The area was then expressed as a percentage of the total area of the 75° FOV, less the area of the sun mask.

5. Evaluation

A total of 592 images were collected during the last 15 days of September 1997. These images had not been previously used in the training program. They were also visually inspected to produce the data for evaluation. Four general rules were applied when determining the degree of solar obstruction in the following special circumstances: if Ci cloud was detected around the sun, its state was classified as DO; if a considerable amount of non-Ci cloud existed near the sun and it was relatively bright in this region, its state was taken as ''disk partially obscured'' (DPO); if it was uncertain whether some pixel were very dark cloud or clear sky around the sun, the state was taken as DPO; and if the sun appeared hazy, then, because this could indicate smoke or other aerosols, but not cloud, the state was recorded as ''disk not obscured'' (DNO).

The results obtained by visual inspection and those obtained by the computer are compared in Table 1. Of the 592 images obtained there were 251 DO, 118 DPO, and 223 DNO. There were also 27 images that were recorded as Ci cloud. Of the 592 images, there were 453 (or 76.5%) correctly identified by the algorithm for the degree of solar obstruction and 485 (or 81.9%) correctly identified for cloud amount based on the categories of overcast (100%–80%), broken (80%–50%), scattered (50%–1%), and clear sky (1%–0%). For DNO cases (223 images), 188 (or 84.3%) were identified correctly for the degree of solar obstruction and 180 (or 80.7%) for cloud amount.

Figure 8 shows the results for 11 September 1997. The vertical axes consist of the calibrated UVB radiation in units of milliwatts per square centimeter on the left scale, the computer derived degree of solar obstruction (0, 0.5, 1, right scale) and cloud amount (%, far right scale). The horizontal axis is given for 6-min intervals between 0917 LT (data point 1) and 1435 LT (51). This day was chosen from the training set, in which case the visual observations matched the computer results and no Ci clouds were present. It was also a day of variable cloud conditions. The ozone reading around noon for this day (as recorded in Brisbane) was 287 DU. The graph of Fig. 8 clearly demonstrates the variation of UVB level with changes in the degree of solar obstruction by cloud and cloud amount around the sun during the day. In one case [between 1112 LT (20) and 1130 LT (23)] there is a general trend in which the UVB level decreased as the cloud cover increased. UVB decreased by 76.6% as the degree of solar obstruction changed from DNO to DO and the cloud amount also increased

from 0% to 100% around the sun. Between 1148 LT (26) and 1154 LT (27) the degree of solar obstruction changed from DO to DPO, with a decrease of cloud amount from 100% to 11%. The corresponding increase of UVB was 65.3%.

A problem of solar reflections on the camera was introduced in the SCSC as a result of the camera being centered on the sun. An example of this can be seen in the top region, just left of the sun, in Fig. 4. This also occurs in other sky camera systems (not concerned with the degree of solar obstruction), in which no shading disk is used to block out the sun in the images. For cloud amount values typically less than 10%, these reflections may be interpreted as small cloud patches. By changing the thresholding levels used for determining cloud pixel for a range of solar radiation readings, this problem is reduced. Other methods of overcoming this problem will be addressed in the next version of the SCSC.

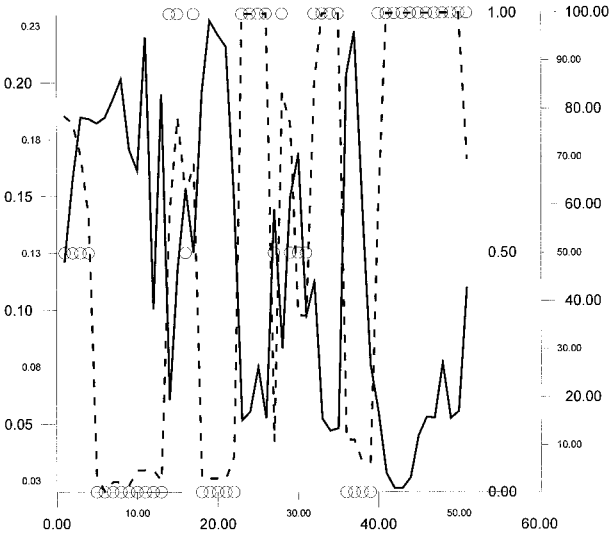

FIG. 8. Results for the 11 Sep 1997 of UVB radiation (———) (mW cm^{-2} left scale), the degree of solar obstruction (○) (0, 0.5, 1 right scale), and cloud amount (– – –) (%, far right scale). It is given for 6-min intervals between 0917 LT (1) and 1435 LT (51); (30) is the first 6-min interval before noon.

6. Conclusions and discussion

A new ground-based sky camera system has been evaluated. It is the first sky camera system to be used for the assessment of cloud conditions in the vicinity of the sun and to automatically retrieve the degree of solar obstruction. Its features include sun tracking, integrated radiation received at the same location, use of solar radiation data, and nonlinear thresholding in the image-processing procedure.

The evaluation of the system for images during September 1997 suggests that the SCSC system can determine the degree of solar obstruction (DNO, DPO, and DO) to an accuracy of about 80%. It can also determine the cloud amount in an FOV of between 25° and 75° of the sun to an accuracy of 80%. This would indicate that the system may have potential to automatically analyze sun-centered sky images for other months of the year.

As seen in Table 1, the SCSC does not handle the detection of DPO or cloud amount between 50% and 80% acceptably at this stage. This is mainly a result of Ci cloud and in some cases very dark cloud. Dark clouds require lower thresholds and thin Ci clouds require higher thresholds. In a future version of the SCSC algorithm, it is proposed to use a similar method as Harris and Barrett (1978) used for satellite cloud images for meteorological purposes. They used a combination of brightness and texture measurements to determine cloud type. Texture is evaluated by measuring the SD as well as the vector dispersion of the density values within small window areas of the whole image. Discriminant analysis scheme windows could then be allocated to Ci, dark, other cloud, or no cloud. The results of their analysis of visible and infrared images showed an accuracy of greater than 72% in cloud type identification. One disadvantage of introducing such a scheme would be a considerable increase in image-processing execution time per image.

The example cloud and UVB data that has been presented clearly illustrates the potential of the system to be used in researching the characterization of the effect of cloud around the sun on UV radiation received at the earth's surface. Generally UVB levels changed as expected in relation to the observed cloud conditions. In some cases UVB changes occurred without corresponding changes in the degree of solar obstruction or cloud amount, as defined in this paper. Such a case is at 1130 LT (23) to 1142 LT (25), in which a 30% increase in UVB occurred for a constant DO and 100% cloud amount during this time. Such cases could be due to variable cloud thickness, changes of cloud conditions during the 6-min data retrieval interval, local changes in tropospheric ozone or aerosols or changes in cloud conditions outside the FOV of the SCSC. A detailed analysis with additional cloud parameters will require further data.

Acknowledgments. We would like to thank the technical staff of both USQ and Queensland University of Technology for construction of the mechanical components, electrical wiring, computer support, and for general assistance with the SCSC. Thanks to Dr. Alfio Parisi for assistance with the spectroradiometer and Professor John Billingsley, both of USQ, for advice on image processing. Also, our thanks to Dr. Jim Easson of the Australian Bureau of Meteorology for supplying the Brisbane ozone data.

APPENDIX A

Degree of Solar Obstruction Algorithm

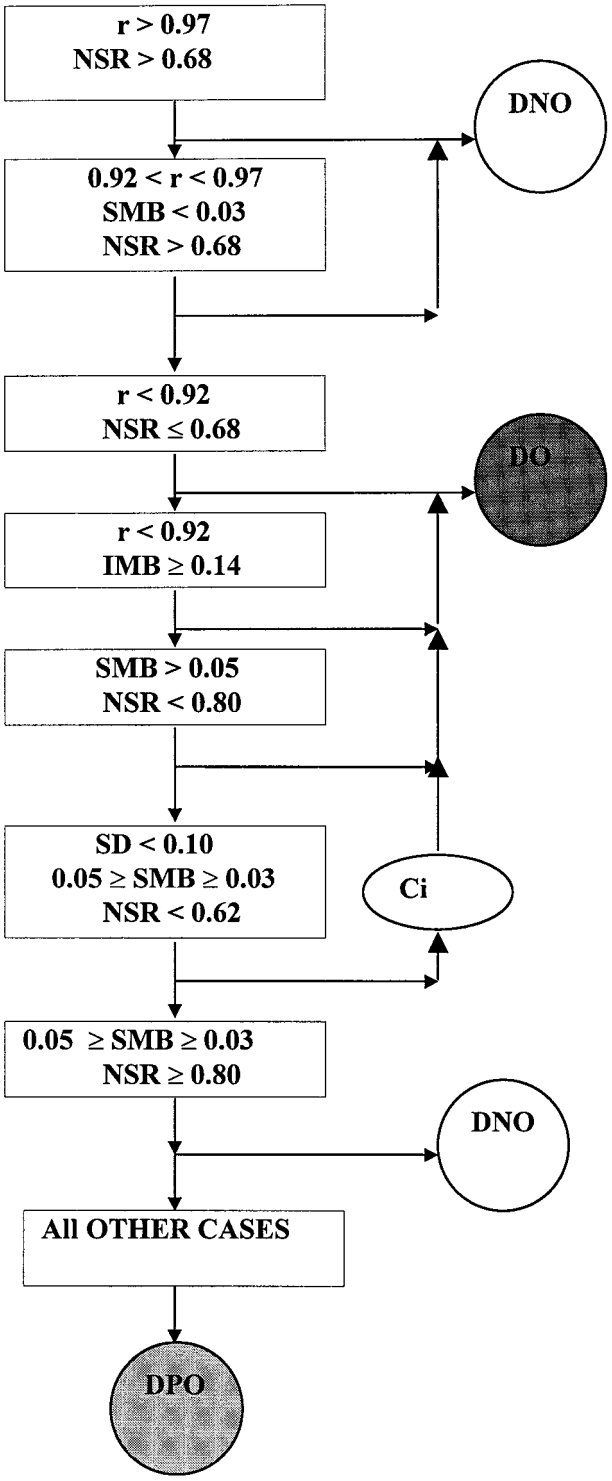

APPENDIX B

Threshold Conditions for Cloud Amount around the Sun

TABLE B1. Threshold conditions.

Disk status	IMB condition	Threshold (%)	Images
DNO	≥0.06	60	2
	<0.06	40	2
DPO	<0.05	35	2
	≥0.05	35	1 & 2
DO	<0.05	10	1 & 2
	≥0.05	20	1 & 2
	<0.05	20	2

REFERENCES

Arrick Robotics, 1995: MD-2 dual stepper motor system user's guide, revision D. Arrick Robotics, 107 pp. [Available from Arrick Robotics, P. O. Box 1574, Hurst, TX 76053.]

Borkowski, J., A.-T. Chai, T. Mo, and A. E. O. Green, 1977: Cloud effects on middle ultraviolet global radiation. *Acta Geophysica Polonica,* **25**(4), 287–301.

Davis, G. B., D. J. Griggs, and G. D. Sullivan, 1992: Automatic estimation of cloud amount using computer vision. *J. Atmos. Oceanic Technol.,* **9,** 81–85.

Digital Vision, 1992: ComputerEyes/RT color frame grabber for IBM PC computers owner's manual, 2d ed. Digital Vision Inc., 120 pp. [Available from Micronica, 184 Napier St., South Melbourne, Victoria Australia.]

Goodman, A. H., and A. Henderson-Sellers, 1988: Cloud detection and analysis: A review of recent progress. *Atmos. Res.,* **21,** 203–228.

Harris, R., and R. C. Barrett, 1978: Toward an objective nephanalysis. *J. Appl. Meteor.,* **17,** 1258–1266.

Monitor Sensors, 1989: Automatic weather monitoring stations installation and operating manual. Monitor Sensors, Australia, 53 pp. [Available from Monitor Sensors, P. O. Box 1178, 7-9 Industry Dr., Cabooltune, Old 4510 Australia.]

Nautical Almanac Office, 1985: *The Astronomical Almanac for the Year 1985.* U.S. Government Printing Office.

Nunez, M., B. Forgan, and C. Roy, 1994: Estimating ultraviolet radiation at the earth's surface. *Int. J. Biometeor.,* **38,** 5–17.

Sabburg, J., and J. Wong, 1997: Development of a sun centered sky camera for use in UV measurements. *Proc. Int. Workshop (IAIF'97),* Adelaide, Australia, Cooperative Research Centre for Sensor Signal and Information Processing (CSSIP), 113–118.

Schafer, J. S., V. K. Saxena, and J. J. De Luisi, 1996: Observed influence of clouds on ultraviolet-B radiation. *Geophys. Res. Lett.,* **23**(19), 2625–2628.

Thompson, C. M., and L. Shure, 1995: Image-processing TOOLBOX for use with MATLAB. The MATH WORKS Inc., 301 pp. [Available from The Math Works, Inc., 24 Prime Park Way, Natick, MA 01760-1500.]

Wong, C. F., S. Toomey, R. A. Fleming, and B. W. Thomas, 1995: UV-B radiometry and dosimetry for solar measurements. *Health Phys.,* **68,** 175–184.

Wooldridge, C., 1993: The development and evaluation of a digital whole-sky cloud monitoring system. Ph.D. thesis, Macquarie University, 303 pp.